Propagation of high-frequency surface plasmons on gold

R. E. Peale,[1,2,*] O. Lopatiuk,[1] J. Cleary,[1] S. Santos,[1] J. Henderson,[1] D. Clark,[1] L. Chernyak,[1] T. A. Winningham,[1] E. Del Barco,[1] H. Heinrich,[1,3] and W. R. Buchwald[4]

[1]*Department of Physics, University of Central Florida, Orlando, Florida 32816, USA*
[2]*College of Optics and Photonics (CREOL), University of Central Florida, Orlando, Florida 32816, USA*
[3]*Advanced Materials Processing and Analysis Center (AMPAC), University of Central Florida, Orlando, Florida 32816, USA*
[4]*Air Force Research Laboratory, Optoelectronic Technology Branch, Hanscom Air Force Base, Massachusetts 01731, USA*
[*]*Corresponding author: peale@mail.ucf.edu*

Received March 4, 2008; revised June 9, 2008; accepted August 5, 2008; posted August 12, 2008 (Doc. ID 93333); published September 24, 2008

Propagation of surface plasmons on gold in the range 2.8–3.5 eV over 0.1–1.6 μm distances was characterized by cathodoluminescence spectroscopy. Surface plasmons were excited by an electron beam near a grating milled in the gold. The spectra of outcoupled radiation reveal increasingly strong propagation losses as surface plasmon energy increases above 2.8 eV, but little effect in the range 1.6–2.8 eV. These results are in partial agreement with theoretical expectations. © 2008 Optical Society of America

OCIS codes: 240.6680, 250.5403.

1. INTRODUCTION

Propagation of electromagnetic signals on metal waveguides via highly confined, bound electromagnetic waves known as surface plasmon polaritons (SPPs) is central to nanophotonics applications that are the subject of current interest [1,2]. Plasmon-electronic integrated circuits (PEIC) have been proposed [3], but the usual optical inputs and outputs for PEIC automatically invoke bulky sources (lasers), coupling structures (prisms, gratings, lenses, fiber), spectrometers, and detectors, which cancel the touted advantages of subwavelength confinement for SPPs. A potentially more compact method of plasmon excitation would be *electrical* SPP generation and detection, e.g., by electron bombardment using nanotube field emitters. The spectrum of electron-beam excited SPPs on metals is concentrated at high visible and ultraviolet energies, where for metals both field confinement and propagation losses are high. Although the characteristic propagation length generally decreases with energy for free-electron metals, gold specifically has a propagation length that is expected to remain constant at about 0.3 μm above 2.5 eV (see below). Thus, electron-beam excited, high-frequency SPPs on gold are potentially interesting for nanoscale PEIC applications.

Use of a scanning electron microscope (SEM) and cathodoluminescence (CL) to study SPP decay for 1–10 μm propagation lengths at energies below 2.3 eV was recently described [4–6]. This paper reports an independent experiment of the same type, but where the main effects occur at SPP energies above 2.8 eV.

2. EXPERIMENT

A nominally 470 nm thick layer of gold was electron-beam evaporated onto a 5 nm Cr sticking layer on a polished silicon substrate. This thickness is sufficient that the optical constants are those of bulk gold. Using a 30 keV focused gallium-ion beam [FEI-200-TEM focused ion beam (FIB) system], several 20 line gratings were cut in the gold with nominal groove length 50 μm, groove depth 50 nm, grating period $a=600$ nm, and different groove widths t. The Fig. 1 inset presents an FIB micrograph of one of the gratings, where all 20 lines appear in the upper part of the image. Analysis of Fig. 1 indicates actual groove length=57 μm, $a=407$ nm, and $t=97$ nm. FIB imaging with a 100 pA gallium beam ablates the surface in a $\sim$100 μm$\times$100 μm region, and this affects the strength of the background cathodoluminescence.

Atomic force microscopy (AFM) images show that the as-evaporated surface consists of circular bumps of 1–4 nm height, 50 nm width, and $\sim$50 nm average separation. The curve in Fig. 1 presents an AFM image slice for the grating. The groove depth is at least 30 nm, but the sharpness and depth of the grooves are degraded by the AFM tip size [7,8]. The grating period, within a few percent accuracy, is 360 nm, which is within 10% of the value from the FIB image. Figure 1 also reveals that the regions between the grooves have been collaterally milled and are lower than the surrounding unstructured gold by about 17 nm.

A Philips XL30 SEM with an integrated Gatan MonoCL3 system collects position dependent CL spectra. An off-axis parabolic aluminum mirror collects $\sim$75% of all light emitted from the vicinity of the excitation. The electron beam transits a 1 mm aperture in the mirror to excite SPPs at the mirror focus. Collection system dimensions sufficiently exceed SPP propagation lengths such that SPP outcoupling occurs essentially at the focus. Emission is directed through a light guide to a

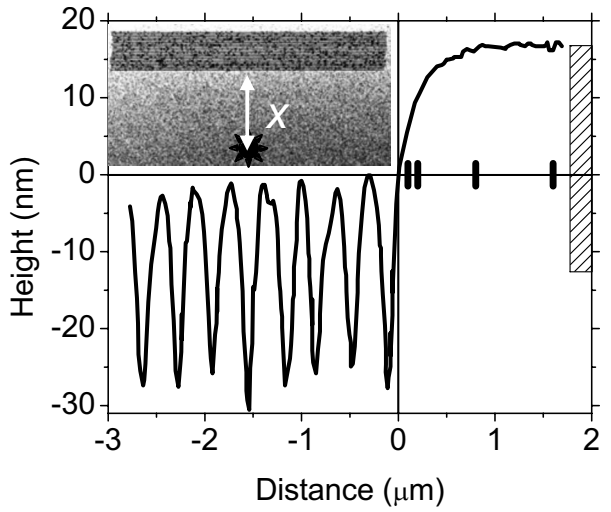

Fig. 1. Atomic force microscopy line scan of grating on gold film. The inset is a focused ion beam micrograph of the grating. The black star schematically represents the ~5 nm diameter electron beam spot (exaggerated for clarity) at a distance x (also exaggerated) from the rulings. CL spectra were collected as a function of x. The bar symbols on the zero line indicate the x values probed. The shaded box represents the penetration depth of the surface plasmon fields into the metal.

Czerny–Turner monochromator (f4.2, 30 cm focal length, 1200 lines/mm grating, 500 nm blaze). The photomultiplier at the spectrometer output is sensitive in the 200–850 nm range. The system spectral response function is known.

The Fig. 1 inset schematically indicates the electron-beam spot at a distance x from the grating. The electron-beam spot is in reality only ~5 nm across, i.e., at least 100 times smaller than its representation. The electron beam excites surface plasmons with a certain frequency distribution and with an efficiency of order of 1% or less [4,9]. SPPs propagate away from the excited spot, and those that reach the grating are coupled into free electromagnetic waves with an efficiency that depends on wavelength and grating geometry [10]. CL spectra were collected at each of several positions x in the range 0.1–1.6 μm. The distance x in the Fig. 1 inset is exaggerated: the maximum x value in the experiment corresponds to just 4 grating periods. Vertical bar symbols on the zero line of Fig. 1 indicate the actual x positions probed.

3. THEORETICAL CONSIDERATIONS

Quantitative discussion of fundamental properties for gold relevant to electron-beam excitation of SPPs and their propagation is presented first. The complex SPP wave vector, for the vacuum metal interface, is determined from the complex permittivity ε of the metal, according to $k=(\omega/c)\sqrt{[\varepsilon/(1+\varepsilon)]}$, where ω is the angular frequency, and c is the speed of light. Empirical permittivity data for gold [11] were used to obtain the dispersion relation ω versus Re[k] that is compared with the light line in Fig. 2. Other permittivity data [12–14] give essentially the same results both here and below. Several labeled ticks on the right axis indicate corresponding optical

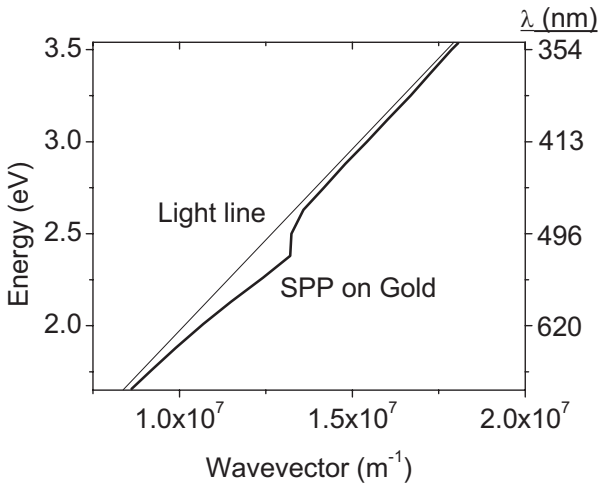

Fig. 2. Comparison of the dispersion relation for SPPs on gold with the light of slope c. The tick labels on the right of the graph indicate the wavelengths of free space radiation that the SPPs would be outcoupled to by the grating.

wavelengths, where the total plotted range is that of the CL experiment. Between 2 and 2.5 eV (620–500 nm wavelength), the SPP dispersion curve falls noticeably below the light line. Above 2.5 eV, rather than leveling off at an SPP resonance frequency as for ideal free-electron metals, the dispersion curve for gold doubles back toward the light line while remaining below it. The fundamental condition for SPPs that Re[ε]<0 remains valid up to at least 5 eV.

The characteristic propagation length L for SPP intensity is $L^{-1}=2\,\mathrm{Im}[k]$. Figure 3 presents calculated L values using permittivity from [11] over the experimental wavelength range, where 0.3 μm$<L<$40 μm. Note especially that for energies above 2.5 eV (below 500 nm optical wavelength), L remains above 0.3 μm. The symbols indicate distances x probed in the experiment.

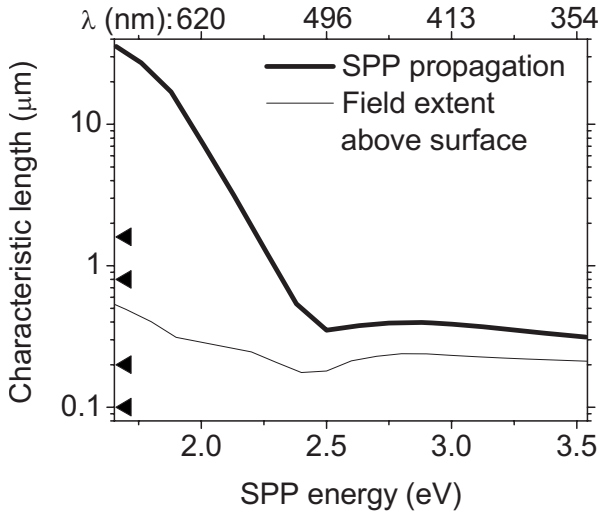

Fig. 3. Characteristic lengths as a function of SPP energy. The propagation length for SPPs on gold is given by the heavy curve. The light curve shows the extent to which SPPs penetrate into the air above the surface. The triangle signals indicate the various distances from the grating that SPPs were excited by the electron beam. The tick labeling on the upper border indicates the photon wavelengths for outcoupled SPPs.

The SPP fields extend above the surface and penetrate into the gold by amounts $L_{\mathrm{Air}}=(c/\omega)/\mathrm{Re}[\sqrt{(-1/(1+\varepsilon))}]$ and $L_{\mathrm{Au}}=(c/\omega)/\mathrm{Re}[\sqrt{(-\varepsilon^2/(1+\varepsilon))}]$. L_{Air} values in the experimental energy range are plotted in Fig. 3 and fall between 0.2 and 0.6 μm. Values for L_{Au} are between 25 and 40 nm, and the shaded box in Fig. 1 schematically indicates the value at 3.5 eV. Thus, the comparatively small ~17 nm recess of the grating below the surface should not prevent the SPP from interacting with the grating, so that outcoupling should proceed in the usual way. However, the spectral efficiency for outcoupling may be very different from that of the gratings in [4–6].

The outcoupling angle θ depends on the characteristic length a of the surface corrugation. The relation between $\mathrm{Re}[k]$ and θ for emission at wavelength λ is

$$\mathrm{Re}[k]=(2\pi/\lambda)\sin\theta+2\pi m/a, \tag{1}$$

where m is a positive integer. Figure 4 plots θ versus λ for SPPs that approach a 360 nm period grating on gold. Positive (negative) angles indicate emission for which the in-plane component of photon momentum is in the same (opposite) direction as the SPP momentum. Contributions from $m=2$ can occur only at the shortest wavelengths, and real solutions for $m=1$ disappear before λ reaches 750 nm. The shaded bars indicate the range of angles that would miss the optimally aligned parabolic collector. In fact, mirror orientation with respect to the grating was neglected during the experiments. In the worst case the shaded boxes in Fig. 4 would be interchanged such that none of the $m=2$ emission and only $m=1$ emission below 640 nm would be collected. For $a=50$ nm, the characteristic length scale of surface roughness, there are no real solutions to Eq. (1) in the wavelength range of the experiment, so that contributions to the background from outcoupling by roughness should be weak. For wavelengths of ~500 nm and below, the SPP propagation length (Fig. 3) is less than the grating period, making the outcoupling angle ill defined. The step edge discontinuity that precedes the grating (Fig. 1) should contribute to outcoupling with a broad angular distribution.

The probability of SPP excitation by electron beams peaks at the SPP resonance frequency $\omega=\omega_p/\sqrt{2}$ for free-electron metals [15]. Experiment [16] and simulation [17] reveal *two* peaks in the electron energy loss spectrum for gold that are attributed to SPP generation. These peaks occur near 2.8 and 5.7 eV as indicated by symbols in Fig. 5. The SPP resonance frequency determined by $\varepsilon=-1$ [18] corresponds to peaks in the function $\mathrm{Im}[-1/(\varepsilon+1)]$, which is usually taken as giving the spectrum of electron energy loss associated with SPP generation [9]. This function indeed shows peaks near the 2.8 and 5.7 eV (Fig. 5).

Next, theoretical considerations relevant to the analysis of the experimental data are presented. The measured emission spectrum $I(x,\lambda)$ with position dependent background spectrum $B(\lambda)f(x)$ is

$$I(x,\lambda)=S(\lambda)\{B(\lambda)f(x)+D(\lambda)G(\lambda)A(\lambda)\exp[-x/L(\lambda)]\}, \tag{2}$$

where S is the known spectrometer response function, D is the distribution of electron-beam excited SPPs, G is an outcoupling efficiency function, and A is a light collection function. These functions will be discussed next.

It is usually assumed [4–6] that the background spectrum has the same intensity at all locations x. It is reasonable to suppose, however, that the background intensity might increase with distance from the grating as surface modification by the FIB decreases. Hence we introduce a position dependent background $B(\lambda)f(x)$, where $f(x)$ is close to but generally less than unity. We take $f(x)=1$ for $x>100$ μm, the typical maximum extent of surface processing by the FIB, and we anticipate that $f(x)$ decreases as the e-beam approaches the grating.

The function $D(\lambda)$ in Eq. (2) is the distribution of surface plasmons at frequency ω excited by the electron beam. Following usual practice [9], this is taken to be the function $\mathrm{Im}[-1/(\varepsilon+1)]$, as plotted in Fig. 5. It is observed

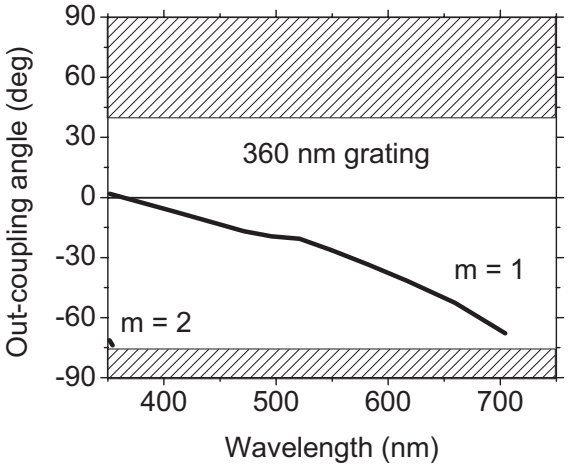

Fig. 4. SPP outcoupling angles for wavelengths in the range of the CL experiment for a grating outcoupler with 360 nm period. The curves for different m values are for corresponding amounts of momenta given up by the SPP to the grating. Negative angles correspond to outcoupled photons with in-plane momentum opposite to that of the SPP. The unshaded part of the figure indicates the range of angles that are collected by the CL apparatus.

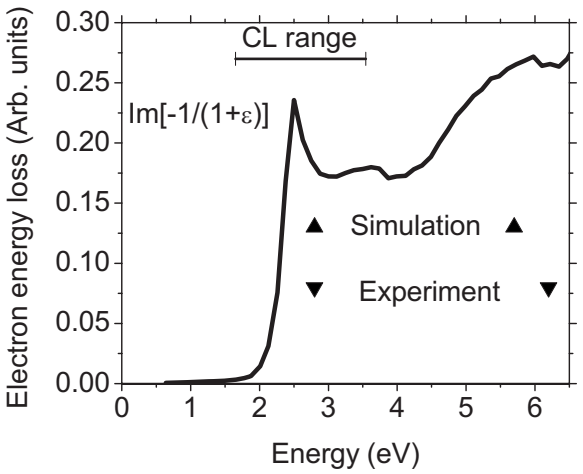

Fig. 5. Electron energy loss spectrum for generation of SPPs on gold. The symbols represent experimentally observed [16] and simulated [17] energy loss peaks. The curve is the energy loss function calculated from the permittivity. The range of photon energies collected by the CL experiment is indicated by the horizontal bar.

to fall sharply for energies below 2.5 eV to the level of only a few percent of the peak at the long wave limit of the experiment.

The function $G(\lambda)$ is the efficiency with which the grating outcouples SPPs into light. This function depends on the geometry of the grating grooves and the wavelength [9], but for simplicity, we take $G(\lambda)=1$ in the analysis of the results.

The function $A(\lambda)$ is the acceptance function of the optical collection system, which occurs because of the anisotropic SPP outcoupling (Fig. 4). The actual angular distribution in the range 350–500 nm should be broad, since here the propagation length is comparable to a single grating period, which suggests that $A(\lambda)$ should increase with λ For simplicity, however, $A(\lambda)=1$ will be assumed.

The method of analysis in [4–6] was to subtract the background spectrum. The difference spectrum, corrected for the system response $S(\lambda)$, is

$$\Delta(x,\lambda) \equiv [I(x,\lambda) - I(x \gg L,\lambda)]/S(\lambda)$$
$$= B(\lambda)[f(x) - 1] + D(\lambda)\exp[-x/L(\lambda)]. \quad (3)$$

For $\lambda > 650$ nm, the second term is x independent, since here the exponential factor is approximately unity for the range of x values probed. Moreover, the function D is comparatively small in this region (Fig. 5), while the measured background is large. The function $\Delta(x,\lambda)/B(\lambda)$ for $\lambda > 650$ nm should therefore define the value of $f(x)-1$. In principle, the experimental Δ values can then be corrected by subtracting the (negative) function $B(\lambda)$ $[f(x) -1]$ to give $D(\lambda)e^{-x/L(\lambda)}$, which can be compared with theory. In our experiment, however, the SPP effects are weak compared to the background, such that the first term in Eq. (3) dominates the experimental results. Therefore, the prescribed method of recovering $D(\lambda)e^{-x/L(\lambda)}$ depends sensitively on precise knowledge of $f(x)$, and analysis of the difference proves impractical.

Instead, analysis of the ratio is preferred in the case of strong background. The ratio of spectra collected at x to a reference spectrum at $x \gg L$ is

$$R(x,\lambda) \equiv I(x,\lambda)/I(x \gg L,\lambda) = f(x) + [D(\lambda)/B(\lambda)]e^{-x/L(\lambda)}. \quad (4)$$

The first term is nearly unity for all x. The second term is small compared with unity, and becomes rapidly smaller with increasing λ due to the factor D/B. When $\lambda > 650$ nm, the second term takes the small x-independent value D/B, so that the function $f(x)$ is approximately defined by experimental $R(x,750\ \text{nm})$ values. This procedure overestimates each $f(x)$ value by the same small term D/B. The experimental ratio spectra $R(x,\lambda)$ are corrected by adding to each of them the positive number $1-f(x)$. Each such corrected ratio is underestimated by the same small amount D/B.

Comparing Eqs. (3) and (4), we find $\Delta = B\ (R-1)$. The relative uncertainty for the difference is much greater than that for the ratio, since $d\Delta/\Delta = dR/(R-1) \gg dR/R$ (experimentally $R \sim 1$). These considerations support the suggestion that in the presence of large background it is better to analyze the ratio than the difference.

4. RESULTS

Experimental ratios of CL spectra are presented in the upper part of Fig. 6 for two distances x. The denominator was taken at $x \sim 1$ mm, and the data have been smoothed somewhat to clarify the broad trends. Values of $f(x)$ have been estimated from $R(x,750\ \text{nm})$ according to Eq. (4), and as expected they were found to be slightly less than unity and to decrease as x decreases. The ratios presented here have already been shifted upwards by the small amounts $1-f(x)$ so that all curves have unity value at 750 nm. At $x = 100$ nm, the shortwave emission dominates. At $x = 1600$ nm, the emission for $\lambda < 450$ nm drops to the level of the background, while the longer wave emission remains strong.

The lower part of Fig. 6 presents calculated ratios for the same two distances. The factor D/B (whose units are arbitrary) has been scaled for better comparison with experiment. The calculated ratios adequately reproduce the observed drop in the ratio values for $\lambda < 400$ nm. The calculated ratios for different x all converge to unity for $\lambda > 700$ nm as seen in the data. However, the drop with x between 400 and 700 nm is less rapid, or even nonexistent in comparison with the calculated effect.

Figure 7 presents a plot of the experimental ratios for three different wavelengths as a function of distance. The heavy curve is the calculated ratio at 350 nm, and the calculated curves for other wavelengths are similar. At 350 nm, the experimental ratio drops rapidly to unity in agreement with the calculation within the experimental uncertainty. However, at 450 nm the experimental ratio hardly changes at all, which is significantly different than the calculation.

Figure 8 presents ratios that reveal an effect of grating geometry. In these ratios the numerator is a spectrum

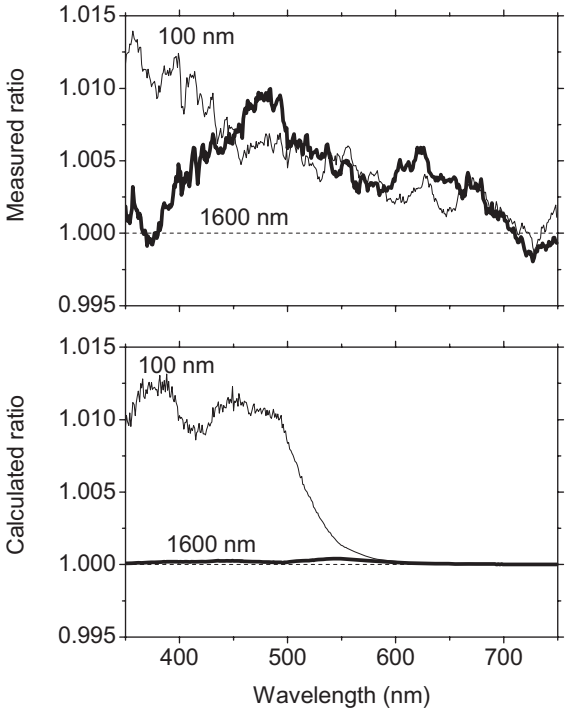

Fig. 6. Measured (top) and calculated (bottom) ratios of CL spectra. Data for two different distances of electron-beam excitation spot from the grating outcoupler are plotted.

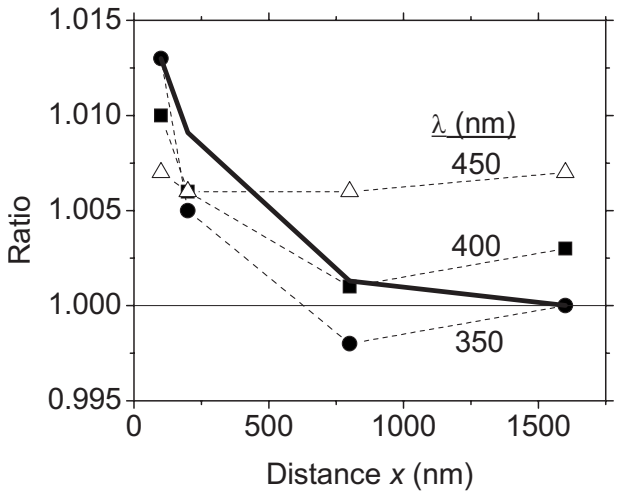

Fig. 7. Ratios of CL spectra at three wavelengths (symbols) as a function of the distance of the electron-beam excitation spot from the grating outcoupler. The heavy curve is calculated ratio for $\lambda = 350$ nm. Calculated curves for other wavelengths are similar.

taken for small x such that sufficient generated SPPs reach the grating. The denominator is a reference spectrum taken at large $x = 100\ \mu\text{m} \gg L$. The two curves are for different gratings with different ratios of groove width to period as indicated. These data suggest that the outcoupling efficiency $G(\lambda)$, is larger for the more asymmetric grating, in agreement with [10].

5. DISCUSSION

The disagreement between measured and calculated ratios (Fig. 6) in the middle of the spectral range has a number of possible explanations. The propagations lengths L may differ from those determined from permittivity-based theory (Fig. 3). The assumed form of the SPP generation function D may be unsuitable. The assumption of spectrally flat grating and acceptance functions G and A is certainly an oversimplification. The assumption of position independence for the spectral shape of the background B is unverified.

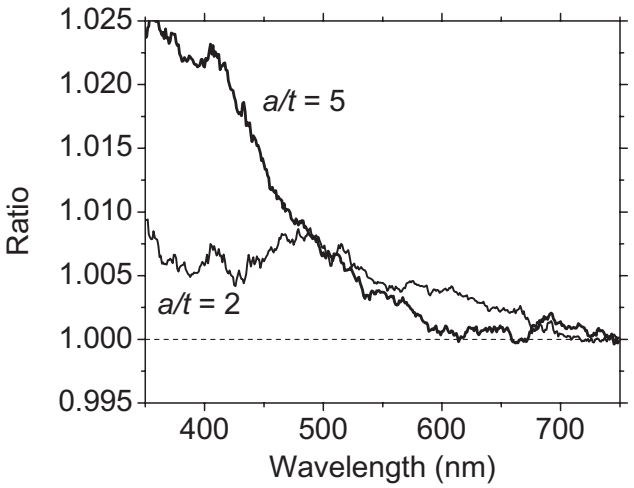

Fig. 8. Ratios of CL spectra for gratings with different ratio of period a (=360 nm) to groove width t.

Propagation lengths are usually found to be about 2–7 times smaller than predicted by permittivity-based theory [4–6]. If L is decreased in Eq. (4), one finds that the calculated ratio of Fig. 6 has more of a hump at 500 nm for the larger distances x. However, these calculated ratios also collapse toward unity even more rapidly with x. Thus, simply scaling the propagation lengths by a constant factor fails to give better agreement. On the other hand, a change in the spectral dependence of L, for example values of L larger than those in Fig. 3 in the spectral region of the discrepancy, would give better agreement with experiment.

In taking $\text{Im}[-1/(\varepsilon+1)]$ for D, we are following [9], which suggests that this function is suitable even when the permittivity is altered by interband transitions as in gold. Also, this function has peaks that agree with those found by energy-loss experiment [16] and simulation [17] and attributed to SPP generation. This function approximates the boundary correction for the plasma loss of fast electrons transmitted by thin foils (Eq. (23) of [15]). However, a D function with larger values in the region near 600 nm would give calculated ratios in better agreement with the experiment.

The previous studies describe their background CL as "significant" [5] or comprising ~75% of the total signal [4]. In our experiment, the differences between spectra near and far from the grating are only about 1%. The origin of the background, and what determines its strength relative to the SPP signal are unclear, though we have argued that SPP outcoupling by surface roughness should be a weak contribution, in contrast to the assumption of [5]. Bashevoy *et al.* [4] attributes the background to d-band emission, dipole radiation originating from incident electrons and their mirror charges, and contaminant fluorescence. This interpretation seems reasonable, although the relative strength of each contribution is difficult to quantify. The theoretical spectral distribution for photons emitted by irradiated metal films peak at both plasmon and interband transition energies [19], whereas our experimentally observed background has a maximum at lower energies in the near IR. Differences in background with [4–6] might be ascribed to differences in electron beam energy, though we note that neither interband transition energies nor plasmon resonance frequencies [20] should depend on this.

To explain the relative weakness of our SPP signal relative to the background, we must suppose that our grating is inefficient at outcoupling SPPs in comparison to those of [4–6]. In [4,6] lines of the grating are raised above the gold surface. In [5], the grating was formed by plasma etching of a Si substrate, later coated in Au, and the tops of the grating bars appear to be level with the gold surface. In contrast, our grating was formed by FIB, which caused the entire grating structure to be sunk by 17 nm below the surrounding surface (Fig. 1), giving a discontinuity in height between surface and grating.

Bashevoy *et al.* [6] found the most efficient outcoupling near 620 nm wavelength for a 400 nm grating and near 840 nm for a 450 nm grating. The corresponding SPP energies are in the tail of the SPP generation curve (Fig. 6). In other words, their $G(\lambda)$ function was strongly peaked within the tail of the $D(\lambda)$ function. That we see evidence

of SPP emission at shorter wavelengths may be due to the specific geometry of our grating, in particular to the step edge discontinuity caused by FIB milling. Differences in grating height cause shifts in the SPP dispersion curve, resulting in a shift in the angular distribution of the outcoupled photons [21], but we judge that this effect is too small to explain the differences between our observations and those of [4–6].

In summary, propagation of electron-beam excited surface plasmons on gold was characterized over 0.1–1.6 μm distances. The effect of attenuation was observed for surface plasmons with energies in the range 2.8–3.5 eV, but not for the lower energies that had been characterized earlier by others. The results are in partial agreement with theoretical expectations. The disagreement is likely due to assumptions made about the spectral dependence of the propagation length, the SPP generation function, the background spectrum, and the grating outcoupling efficiency.

ACKNOWLEDGMENTS

The authors acknowledge funding for this work provided by the Air Force Office of Scientific Research Task 06SN05COR and Air Force Research Laboratory contract FA871806C0076.

REFERENCES

1. M. L. Brongersma and P. G. Kik, *Surface Plasmon Nanophotonics* (Springer, 2007).
2. S. A. Maier, *Plasmonics: Fundamentals and Applications* (Springer, 2007).
3. R. A. Soref, "Introduction—The Opto-Electronic Integrated Circuit," in *Silicon Photonics—The State of the Art*, G. Reed, ed. (Wiley, 2008), pp. 1–14.
4. M. V. Bashevoy, F. Jonsson, A. V. Krasavin, N. I. Zheludev, Y. Chen, and M. I. Stockman, "Generation of traveling surface plasmon waves by free-electron impact," Nano Lett. **6**, 1113–1115 (2006).
5. J. T. van Wijngaarden, E. Verhagen, A. Polman, C. E. Ross, H. J. Lezec, and H. A. Atwater, "Direct imaging of propagation and damping of near-resonance surface plasmon polaritons using cathodoluminescence spectroscopy," Appl. Phys. Lett. **88**, 221111 (2006).
6. M. V. Bashevoy, F. Jonsson, K. F. MacDonald, Y. Chen, and N. I. Zheludev, "Hyperspectral imaging of plasmonic nanostructures with nanoscale resolution," Opt. Express **15**, 11313–11320 (2007).
7. J. Aue and J. Th. M. De Hossona, "Influence of atomic force microscope tip—sample interaction on the study of scaling behavior," Appl. Phys. Lett. **71**, 1347–1349 (1997).
8. E. C. W. Leung, P. Markiewicz, and M. C. Goh, "Identification and visualization of questionable regions in atomic force microscope images," J. Vac. Sci. Technol. B **15**, 181–185 (1997).
9. H. Raether, "Surface plasma oscillations and their applications," in *Physics of Thin Films*, G. Hass, M. H. Francombe, and R. W. Hoffman, eds. (Academic, 1977), Vol. 9, pp. 145–261.
10. A. V. Krasavin, K. F. MacDonald, and N. I. Zheludev, "Active plasmonics," in *Nanophotonics with Surface Plasmons*, V. M. Shalaev and S. Kawata, eds. (Elsevier, 2007), pp. 109–139.
11. P. B. Johnson and R. W. Christy, "Optical constants of noble metals," Phys. Rev. B **6**, 4370–4379 (1972).
12. E. D. Palik, ed., *Handbook of Optical Constants of Solids* (Academic, 1985).
13. M. L. Theye, "Investigation of the optical properties of Au by means of thin semitransparent films," Phys. Rev. B **2**, 3060–3078 (1970).
14. B. Dold and R. Mecke, "Optical properties of noble metals, transition metals, and their alloys in the infrared pt. 2," Optik (Jena) **22**, 453–463 (1965).
15. R. H. Ritchie, "Plasma losses by fast electrons in thin films," Phys. Rev. **106**, 874–881 (1957).
16. J. C. Ingram, K. W. Nebesny, and J. E. Pemberton, "Optical constants of the noble metals determined by reflection electron energy loss spectroscopy," Appl. Surf. Sci. **44**, 293–300 (1990).
17. Z.-J. Ding and R. Shimizu, "Monte Carlo simulation study of reflection-electron-energy-loss-spectroscopy spectrum," Phys. Rev. B **61**, 14128–14135 (2000).
18. E. A. Stern and R. A. Ferrell, "Surface plasma oscillations of a degenerate electron gas," Phys. Rev. **120**, 130–136 (1960).
19. R. H. Ritchie and H. B. Eldridge, "Optical emission from irradiated foils. I," Phys. Rev. **126**, 1935–1947 (1962).
20. N. Yamamoto, K. Araya, and F. J. Garcia de Abajo, "Photon emission from silver particles induced by a high-energy electron beam," Phys. Rev. B **64**, 205419 (2001).
21. D. Heitmann, "Radiative decay of surface plasmons excited by fast electrons on periodically modulated silver surfaces," J. Phys. C **10**, 397–405 (1977).